Plasma Physics Reports, Vol. 30, No. 2, 2004, pp. 121–127. Translated from Fizika Plazmy, Vol. 30, No. 2, 2004, pp. 139–146.

PLASMA DIAGNOSTICS

X-ray Backlighting of the Periphery of an Imploding Multiwire Array in the Angara-5-1 Facility

E. V. Grabovskiĭ, K. N. Mitrofanov, G. M. Oleĭnik, and I. Yu. Porofeev

Troitsk Institute for Innovation and Fusion Research, Troitsk, Moscow oblast, 142190 Russia

Received July 24, 2003

Abstract—Backlighting diagnostics for studying the peripheral region of an imploding liner in the Angara-5-1 facility by using X-ray emission from an X-pinch is described. The spatial resolution of the diagnostics was no worse than 4 μm. The X-pinch emission passed through the plasma was recorded with a photofilm. The plasma density was reconstructed from the photofilm blackening density with the help of a step attenuator made of the same material as the liner. Results are presented from experiments on X-ray backlighting of the peripheral region of a multiwire liner at the 70th ns after the beginning of the discharge. It was found that, by this time, the wire cores were depleted to different extent, their masses totalled 70% of the original wire mass, and their diameters had increased approximately threefold. The plasma ejected from the wire cores was found to be axially stratified with a spatial period of 200 μm. Sometimes the axial nonuniformity of the core material with a characteristic scale length of 20 μm was observed. *© 2004 MAIK "Nauka/Interperiodica".*

1. INTRODUCTION

The current-induced implosion of cylindrical tungsten-wire arrays (liners) has been studied since the late 1980s [1–6]. The high-power soft X-ray pulse generated in the phase of maximum compression and the stagnation of the plasma in the final stage of the liner implosion is used in inertial confinement fusion research and in studying the equations of state of various substances at ultrahigh energy densities.

Knowledge of the time evolution of the mass density distribution inside imploding liners is of great importance for understanding the physics of implosion. One of the methods for determining the absolute value of the mass density in such objects is through plasma backlighting with emission from a point X-ray source. The duration of the X-ray burst from such a source should be much shorter than the characteristic times of the processes occurring in the plasma under study. The data on absorption of the probing radiation are used to determine the plasma density in the liner. An X-ray source for such backlighting can be either a plasma created by a high-power short-duration laser beam focused onto a solid target [7, 8] or an X-pinch burst [9–11].

In this study, an X-pinch source was used for backlighting [12]. The data on the absorption of X-ray emission in the liner plasma was obtained by recording the transmitted emission on a photofilm.

Along with measuring the absorption coefficient in plasma by recording two-dimensional images of the liner on an X-ray film (as in fluorography), this study was also aimed at determining the distribution of the mass density in the peripheral part of a tungsten wire liner in the course of its implosion.

2. EXPERIMENTAL SETUP

A scheme of the experiment on X-ray backlighting of the liner periphery is shown in Fig. 1. The system was adjusted in such a way that the images of both the internal and external regions of the liner were recorded on an X-ray film (i.e., the line of sight passed along the tangent to the cylindrical surface of the array, as is shown in Fig. 1). In our experiments, X-ray films were placed at a distance of 1.2 m from the X-pinch.

The X-pinch array consisted of four crossed 20-μm-diameter Mo wires that were connected at their middle points. The X-pinch array was set in place of one of the eight return-current posts at a distance of 45 mm from the liner axis (see Fig. 2). Therefore, it was connected in series with the main load (liner) of the generator. Consequently, the X-pinch was synchronized with the Z-pinch. The X-pinch emitted more than 200 mJ per burst into a 4π solid angle [13].

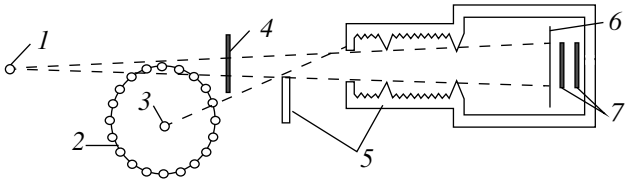

Fig. 1. Scheme of the experiment on X-ray backlighting of the liner periphery: (*1*) X-pinch, (*2*) wire array, (*3*) Z-pinch, (*4*) test wire, (*5*) system of screens and diaphragms, (*6*) foil, and (*7*) X-ray films placed one behind another.

1063-780X/04/3002-0121$26.00 © 2004 MAIK "Nauka/Interperiodica"

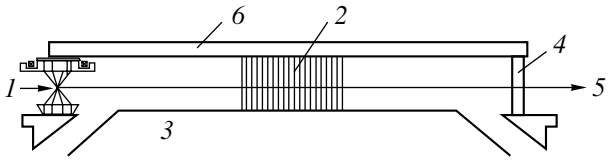

Fig. 2. X-pinch arrangement on the anode disc (side view): (*1*) X-pinch, (*2*) multiwire array (liner), (*3*) liner cathode, (*4*) return-current post, (*5*) to the detector, and (*6*) liner anode.

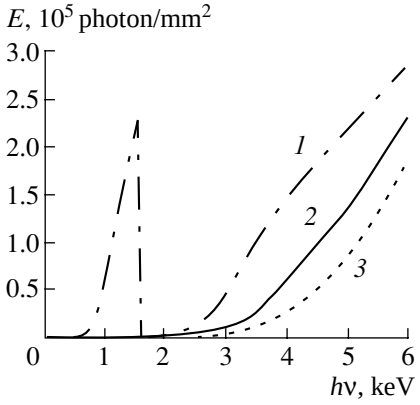

Fig. 3. Spectral sensitivity of a UF-ShS X-ray film placed (*1*) behind a 10-μm Al foil, (*2*) behind a 10-μm Al foil and 100-μm X-ray film, and (*3*) behind a 10-μm Al foil and two 100-μm X-ray films. The sensitivity curves correspond to a film blackening density of $D = 1$.

2.1. Detector of X-pinch Emission

The X-pinch emission was recorded on RF-3 and UF-ShS X-ray films.

The spectral sensitivity and the characteristic curves of the UF-ShS X-ray film were measured in [14]. More detailed information on the UF-ShS X-ray film is presented in [15].

The X-ray films were placed one behind another. The first (RF-3) film recorded an X-ray image created by X rays that passed through a 16-μm Ti foil or 10-μm Al foil. The second film recorded an X-ray image produced by X rays that passed through a metal foil and the first X-ray film with a thickness of 100 μm. Thus, every subsequent X-ray film recorded an image produced by harder X rays than the previous one. In the Angara-5-1 facility, up to four X-ray films were placed one behind another.

The spectral sensitivities of UF-ShS X-ray films placed behind a 10-μm Al foil (curve *1*), behind a 10-μm Al foil and 100-μm X-ray film (curve *2*), and behind a 10-μm Al foil and two 100-μm X-ray films (curve *3*) are shown in Fig. 3. The curves are plotted for a film blackening density of $D = 1$.

2.2. Selection of X-pinch Emission against the Background Z-pinch Emission

A specific feature of the backlighting of multiwire arrays with X-pinch emission is that the Z-pinch is a much more intense source of X-ray emission than the X-pinch. Hence, it can substantially contribute to the detector output signal. When recorded on an X-ray film, this will manifest itself as a parasitic exposure of the film.

In the final stage of implosion, the power of X-ray emission from the Z-pinch reaches 6 TW, the pulse duration is 5–10 ns, and the characteristic photon energy is less than 2 keV. The emission zone, which has a diameter of 0.4–2 mm and height of 1 cm, resides on the axis of the multiwire array [16]. Meanwhile, the power of the X-ray emission from the X-pinch in the photon energy range of 2–20 keV is no higher than 300 MW [13]; i.e., it is lower by a factor of 30000. The ratio between the Z- and X-pinch emission energies (30–80 kJ and 200–700 mJ, respectively) is of the same order of magnitude (actually, somewhat higher). Although the photon energy ranges of emission from the Z- and X-pinches formally do not overlap, there is always a high-energy tail in the Z-pinch emission spectrum. This tail overlaps with the X-pinch emission spectrum, and the power and energy of this tail can be comparable to those of X-pinch emission. In the final stage of implosion, the scattered Z-pinch emission can be also comparable in power to X-pinch emission.

To prevent the X-ray film from exposure to the forward and scattered X-ray emission from the Z-pinch, a set of screens and diaphragms were placed between the Z-pinch and X-ray films (see Fig. 1). The diaphragms also protected the films from exposure to scattered hard X rays. To shield the films from the microparticle flows and radiation arising at the instant of liner pinching, as well as from plasma radiation emitted from the liner periphery, the films were coated with a 16-μm Ti foil or 10-μm Al foil.

2.3. Spatial and Temporal Resolution of the Diagnostics

The instant of the X-pinch burst and its duration were determined using pin diodes. The measurements with pin diodes [13] showed that the full width at half-maximum of the X-pinch emission pulse is ≈1.8 ns in the photon energy range of >2 keV and 1.5 ns in the range of >5 keV. These values characterize the time resolution of X-ray backlighting. The true duration of the X-pinch emission pulse was probably shorter than the measured one because the temporal resolution of pin diodes was ≈1.2 ns; hence, it was not possible to record shorter pulses.

The spatial resolution of the recorded shadowgraphs was determined by several factors. These were diffraction, the refraction of the probing beam in a medium with a variable density, the interference of the deflected

beams, and the finite source dimensions. We estimated the role of diffraction. For this purpose, we calculated the distribution of the relative radiation intensity on the screen set behind an opaque strip of width d. The calculations were performed using the Fresnel method. The emission spectrum was assumed to lie in the range 1–8 keV. The modification of the spectrum by a filter consisting of a 10-μm Al foil and one 100-μm X-ray film placed behind the foil was also taken into account. The distance between the source and the strip was 5 cm, and the distance between the strip and the screen was 1.2 m. The full width at a level of one-half of the sum of the minimum intensity (in the shadow region) and the unperturbed intensity (far enough from the strip shadow) was taken as the width of the diffraction pattern obtained. This width was recalculated to the original object with account taken of the scaling factor. The intensity distribution behind the strip with a thickness of d = 4 μm recalculated to the object is shown in Fig. 4a. The shadow width is Δ = 5.8 μm. The shadow width Δ as a function of d is shown in Fig. 4b. The diagonal in this figure corresponds to a situation in which diffraction is absent and the shadow width is equal to the strip width. It can be seen that the distance between this diagonal and the curve Δ(d) is no larger than 3 μm. Formally, to determine the diffraction-limited spatial resolution, one should find the response for a zero-width strip. However, such a response would be of infinite width. The leftmost point on the Δ(d) dependence has the coordinates d = 1.5 μm and Δ = 4.5 μm. Taking into account the results of the above calculations and the width of the diffraction pattern, the diffraction-limited spatial resolution can be estimated as no worse than 4 μm.

To verify the spatial resolution of the diagnostics and determine the source size, 5-μm test wires (with no current) were placed near the liner under study (see Fig. 1). It can be seen from Fig. 5 that the 5-μm test wire is recorded correctly. This fact, together with the estimated value of the diffraction-limited spatial resolution (4 μm), evidences that the contribution of any of the other factors to the spatial resolution is lower than that of diffraction. This allows us to obtain an upper estimate for the source size. In the case of an X-pinch burst, the source size is less than 4 μm. In [17], the size of an X-ray source on the basis of an X-pinch was found to be less than 2 μm in the photon energy range >4 keV.

To find the relation between the blackening density of X-ray films and the mass density of the liner material, we performed the following calibration procedure. A step attenuator made of the same material as the liner (in our case, tungsten) was placed in front of the X-ray films (this is not shown in Fig. 1). The step attenuator consisted of tungsten filters with surface densities from 300 to 1300 μg/cm^2. The filter shadows in the X-pinch emission were recorded on X-ray films. The surface density of the plasma under study was estimated by comparing the film blackening density measured in the experiment with that obtained in the calibration procedure.

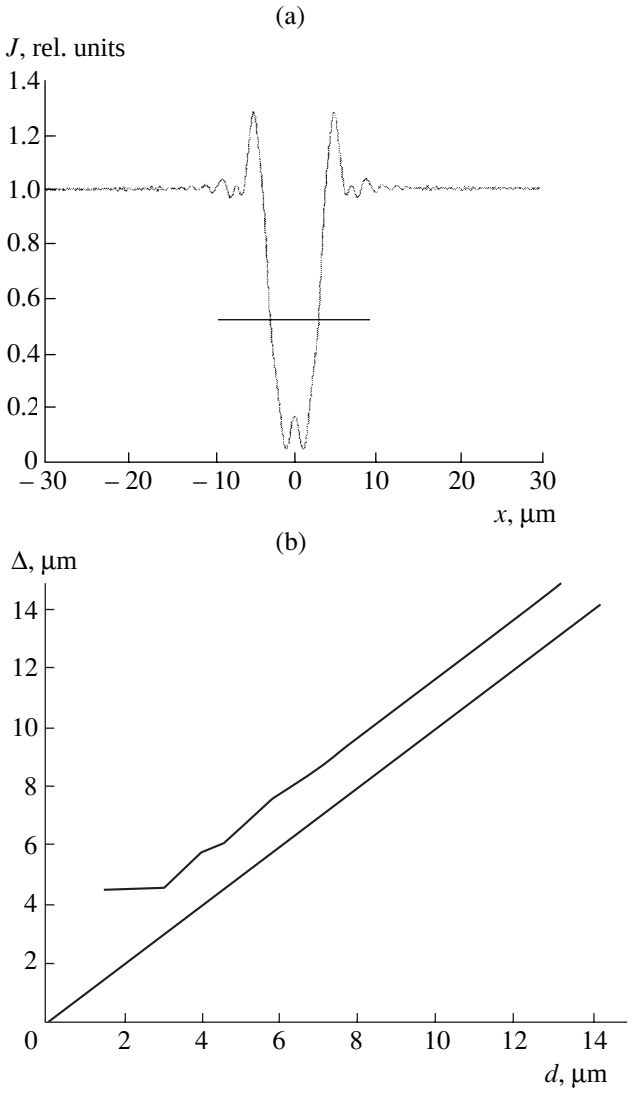

Fig. 4. Simulations of the shadow produced by an opaque strip with allowance for diffraction: (a) the intensity profile $J(x)$ behind the strip with a thickness of d = 4 μm (the profile is recalculated to the object with account taken of the scaling factor; the horizontal straight line shows the ordinate used to determine the shadow width) and (b) the shadow width Δ as a function of the strip width d (the diagonal corresponds to a situation in which diffraction is absent and the shadow width is equal to the strip width). Simulations were performed for the X-pinch emission spectrum (1–8 keV) modified by a filter consisting of a 10-μm Al foil and a 100-μm X-ray film (Fig. 3, curve *2*).

3. BACKLIGHTING OF THE LINER PERIPHERY

The results of the X-ray backlighting of the peripheral region of a multiwire array at t = 70 ns after the beginning of the discharge, when the current per wire had reached 50 kA, are shown in Fig. 5. The liner, 12 mm in diameter and 1 cm in length, consisted of 40

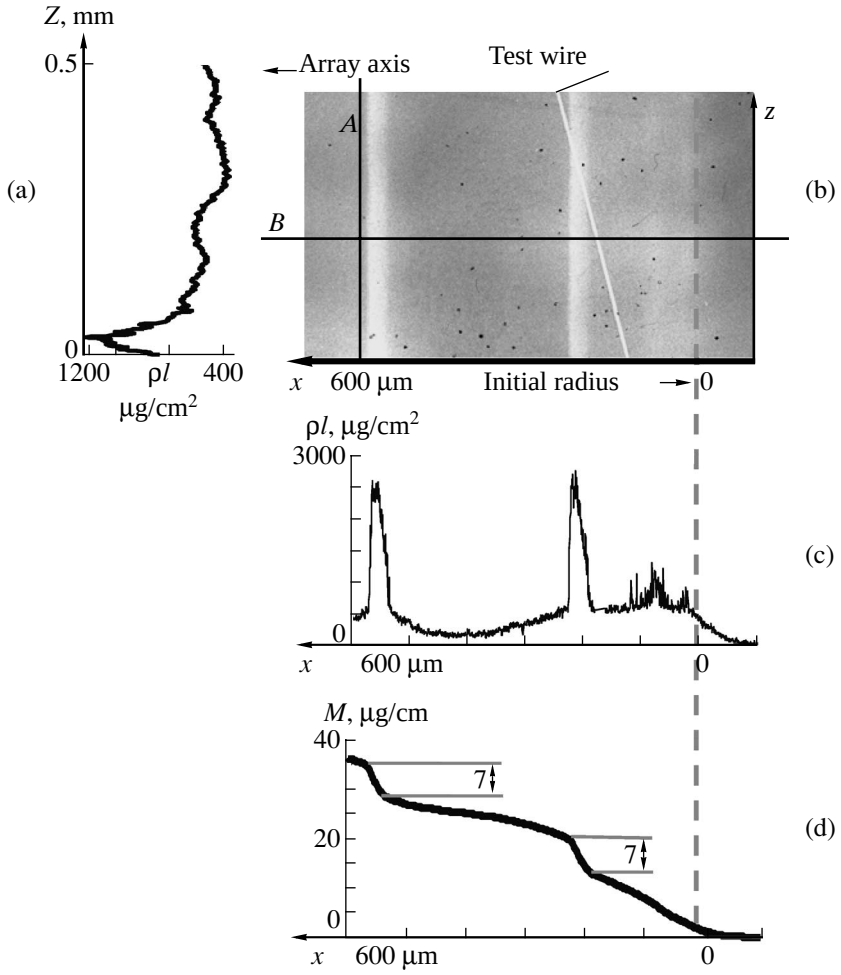

Fig. 5. Mass density distribution in the imploding liner at $t = 70$ ns from the beginning of the discharge: (a) the profile of the surface plasma density along straight line *A*, (b) the shadows of the test wire (slanting line) and dense cores (vertical bands), (c) the profile of the surface plasma density along straight line *B*, and (d) the linear density of the substance located between the outer boundary of the liner and the current *x* coordinate. The liner with a diameter of 12 mm consists of 40 8-μm tungsten wires. The interwire distance is 1 mm. The wire linear density is 9.5 μg/cm.

8-μm tungsten wires with a linear density of 9.5 μg/cm. Figure 6 shows the waveforms of the current through the liner, the power of soft X-ray emission from the Z-pinch, and the X-pinch emission power under conditions corresponding to Fig. 5.

A fragment of a shadowgraph obtained by the backlighting method is shown in Fig. 5b. The results of processing this shadowgraph are shown in Figs. 5a, 5c, and 5d. The *x* and *z* axes in Fig. 5b define the coordinate system that will be used subsequently. The *x* axis is directed along the radius from left to right (toward the array axis), the origin $x = 0$ being at the point with the *r* coordinate corresponding to the initial radius of the wire array. The *z* axis is directed along the liner axis (toward the anode), the origin $z = 0$ being at the bottom of the shadowgraph fragment.

The light slanting line on the shadowgraph fragment is a shadow produced by a 5-μm test wire. At $x = 220$ μm and $x = 550$ μm, one can clearly see the shadows of two dense wire cores.

The shadowgraph of the step tungsten attenuator with a known surface density (this is not shown in Fig. 5b) allowed us to estimate the plasma mass density at different liner points. Below, we will use such a characteristic of the mass density distribution as the surface density ρl [μg/cm²], which is the integral of the plasma mass density $\int \rho dl$ along a straight line *l* passing through the X-pinch and the point with coordinates (*x*, *z*).

The profiles of the surface density ρl along lines *A* and *B* are shown in Figs. 5a and 5c, respectively. In Fig. 5b, line *B* is directed radially and passes at the midheight of the shadowgraph fragment ($z = 0.25$ mm), while line *A* is directed axially and passes at a distance of 5 μm from the left margin of the left dense core ($x = 568$ μm).

In Fig. 5c, the profile of the plasma surface density ρl has two 25-μm-wide peaks (at x = 220 μm and x = 550 μm) corresponding to the shadows of the two dense cores. The diameter of the dense cores is larger than initial wire diameter by a factor of ~3; i.e., 60–80 ns after the beginning of the discharge, the diameter of the liner wires increases nearly threefold. To the right of the dense cores, there are two faint fuzzy peaks (at x = 20 and 80 μm) corresponding to the shadows of the two cores that have evaporated to a much greater extent. In the shadowgraphs, these have almost evaporated, and their smeared cores manifest themselves as variations in the blackening density over the entire length of the initial wires (see, e.g., the shadowgraph fragment presented in Fig. 5b). This fact evidences (i) that smeared cores do exist and (ii) that different wires evaporate to different extent; this could be related to the nonuniformity of plasma production and, perhaps, the nonuniformity of the liner current.

The integral of the plasma surface density ρl [μg/cm^2] from Fig. 5c taken over the x axis,

$$M(X) = \int_{-\infty}^{x} \rho l dx,$$

is shown in Fig. 5d. It is a function of the x coordinate and gives the linear mass density M [μg/cm] of the substance located between the outer boundary of the liner and the current x coordinate. Although the lower integration limit was set at $-\infty$, the integral was actually taken from the outer boundary ($x \sim -100$ μm). The estimated mass remaining in the dense cores with diameters of about 25 μm is ~7 μg/cm. The initial mass of one wire is 9.5 μg/cm; hence, the dense cores contain about 70% of the initial wire mass. The rest of the wire mass is spread out toward the liner axis over a distance of ~200 μm. In the case of smeared cores, the wire mass is spread out toward the liner axis over a distance of ~400 μm. We note that a minor fraction of the plasma is spread outward: a low-density plasma extends to a distance of ~100 μm from the initial boundary of the liner.

In Fig. 5a, which shows the axial profile of the plasma surface density, one can see the axial stratification of the plasma near the core with a period of about 200 μm. At t = 70 ns after the beginning of the discharge, the surface density in these plasma jets is ~1000 μg/cm^2.

In some discharges, we observed the internal axial inhomogeneity of the core itself with a characteristic period of 20 μm (see Fig. 7). It can be seen that there are sites in which the core looks as if it is fractured in the axial direction. In these sites, the mass density is much lower and, perhaps, all the core material has already been transformed into plasma.

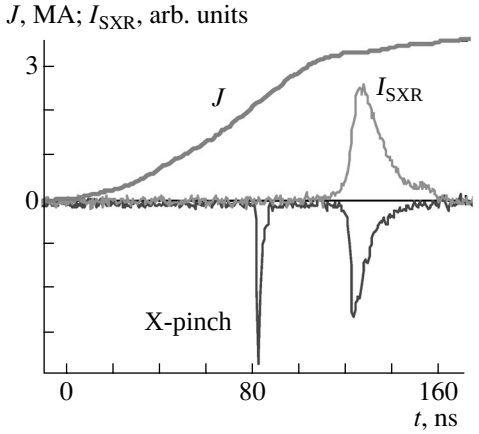

Fig. 6. Waveforms of the liner current J, the intensity of soft X-ray emission I_{SXR}, and the signal from a pin detector sensitive in the range 2–5 keV (the first spike is the X-pinch burst, and the second pulse is the Z-pinch burst) for the parameters of Fig. 5.

Fig. 7. Inner axial inhomogeneity of the core at the instant 60 ns after the beginning of the discharge. The current per wire is 30 kA. The liner with a diameter of 20 mm consists of 60 6-μm tungsten wires; the interwire distance is 1 mm.

4. DISCUSSION

The process of the wire array implosion can be outlined as follows:

Over the first several nanoseconds after the beginning of the discharge, a plasma corona arises near the wire surfaces, and the current switches from the wires to the corona [18, 19]. A further heating of the wires is primarily due heat transfer from the plasma corona. The wire array becomes a heterogeneous system consisting of the dense wire cores and a surrounding low-density plasma. The wire cores consist of a substance with a

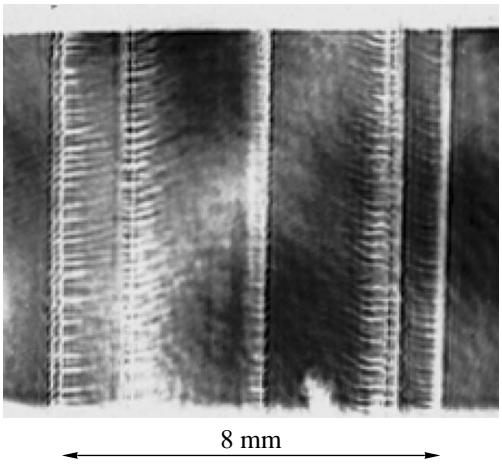

Fig. 8. Wire array shadowgraph obtained by pulsed laser probing at the instant $t = 54$ ns from the beginning of the discharge. The current per wire is 25 kA. The liner of diameter 8 mm consists of 8 6-μm tungsten wires. The characteristic period of axial modulations is 200–300 μm. The characteristic azimuthal size of the plasma jet emerging from the wire in the middle of the figure is no larger than 100 μm.

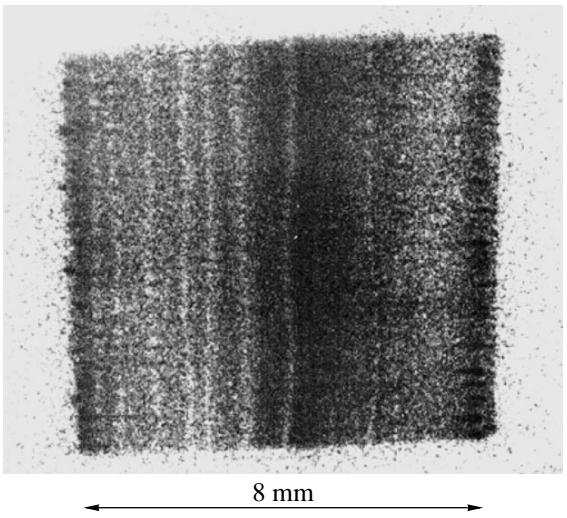

Fig. 9. X-ray frame image of the wire array 20 ns before the Z-pinch burst. The shadows in the prepinch emission are produced by the wire cores surrounded by the plasma corona.

density as high as the density of solids. Over the most part of the discharge, the cores remain in their initial positions and act as stationary plasma sources.

The Ampère force caused by the current flowing through the plasma corona surrounding the wires accelerates the plasma toward the axis of the wire array. The plasma generated on each wire acquires the form of highly nonuniform jets stretched along the radius toward the array axis.

The results obtained allow us to conclude that, by the time $t = 60$–70 ns after the beginning of the discharge, the bulk of the array mass (about 90%) is concentrated at the periphery and only a minor fraction of the low-density plasma has reached the liner axis. The plasma originated from a single wire is spread out toward the liner axis over a distance of ~400 μm. This is less than the liner interwire distance, which is equal to 1 mm. This means that it makes no sense to talk about a plasma shell that implodes as a single entity (at least at the instant $t = 70$ ns after the beginning of the discharge).

The high azimuthal and axial nonuniformity of the plasma flows allowed the authors of [20] to propose the so-called "plasma rainstorm" model. In the Angara-5-1 facility, the fragmentation of the plasma into jets was also recorded by other diagnostics [16, 21].

Figure 8 presents a wire array shadowgraph obtained by pulsed laser probing at the instant $t = 54$ ns after the beginning of the discharge, when the current per wire was 25 kA. The plasma emerging from the wires consists of plasma jets that are modulated in the axial direction and move toward the liner axis (see Fig. 8). The characteristic period of these modulations is 200–300 μm. The characteristic azimuthal size of the plasma jets is no larger than 100 μm (see the wire image in the middle of the figure).

As the array cavity is filled with hot plasma, a prepinch is formed well before the final stage of implosion. The prepinch and the plasma jets are both sources of soft X rays. The cold cores and the plasma corona surrounding them produce shadows in radiation from the prepinch and the plasma jets. Figure 9 presents a shadowgraph of a wire array in the course of implosion. The array consisted of 32 8-μm tungsten wires. The shadows are seen in radiation with photon energies from 0.1 to 1 keV. For this reason, the shadow size is significantly larger than that observed when an X-pinch is used as a radiation source. In different shadowgraphs, the shadow size varies in the range 100–400 μm. Shadows with such dimensions are produced by the plasma surrounding the dense cores. Similar shadows are also seen in the time-integrated X-ray images of an imploding wire liner [21]. We note that the shadows are clearly seen at the left of Fig. 9, whereas at the right, they are not so pronounced. This fact indicates that the wires at the right in Fig. 9 have evaporated to greater extent than those at the left. This may be explained in the same way as in the backlighting experiments (see Fig. 5), namely, by the nonuniformity of the liner current and plasma production.

To determine the fraction of the liner mass that remains at the liner periphery at the instant of the Z-pinch burst (approximately within 100–120 ns after the beginning of the discharge), one needs to either employ other diagnostics (such as laser interferometry [22]) or to shift the X-pinch burst closer in time to the Z-pinch burst.

5. CONCLUSIONS

Thus, the results of X-ray backlighting of a wire array at the 70th nanosecond after the beginning of the discharge can be formulated as follows:

(i) There are dense wire cores with masses of ~70% of the initial wire mass. The rest of the core mass is spread out toward the lines axis over a distance of ~200 μm.

(ii) The diameters of the dense cores are about three times the initial wire diameter. The substance density in the expanded cores is at least one order of magnitude lower than the initial density of the cold tungsten.

(iii) Besides the dense cores, there are also smeared cores that have evaporated to a much greater extent. Their material is spread out toward the axis over a distance of ~400 μm. This fact indicates the nonuniformity of the plasma production and, perhaps, of the liner current.

(iv) The radial size of the region occupied by the material evaporated from the wires is less than the interwire distance.

(v) Outside the liner, the low-density plasma extends to a distance of ~100 μm.

(vi) The plasma on the inner side of the cores is stratified in the axial direction with a period of 200 μm.

(vii) An axial inhomogeneity with a characteristic scale length of 20 μm is observed inside the cores.

REFERENCES

1. M. B. Bekhtev, V. D. Vikharev, S. V. Zakharov, *et al.*, Zh. Éksp. Teor. Fiz. **95**, 1653 (1989) [Sov. Phys. JETP **68**, 955 (1989)].
2. I. K. Aĭvazov, M. B. Bekhtev, V. V. Bulan, *et al.*, Fiz. Plazmy **16**, 645 (1990) [Sov. J. Plasma Phys. **16**, 373 (1990)].
3. T. W. L. Sanford, B. M. Marder, R. B. Spielman, *et al.*, Phys. Rev. Lett. **77**, 5063 (1996).
4. R. B. Spielman, C. Deeney, G. A. Chandler, *et al.*, Phys. Plasmas **5**, 2105 (1998).
5. S. V. Lebedev, F. N. Beg, S. N. Bland, *et al.*, Phys. Plasmas **8**, 3734 (2001).
6. V. V. Alexandrov, I. N. Frolov, E. V. Grabovsky, *et al.*, IEEE Trans. Plasma Sci. **30**, 559 (2002).
7. M. H. Key, P. T. Rumsby, R. G. Evans, *et al.*, Phys. Rev. Lett. **45**, 1801 (1980).
8. D. T. Attwood, IEEE J. Quantum Electron. **14**, 909 (1978).
9. S. V. Lebedev, F. N. Beg, S. A. Pikuz, *et al.*, Phys. Rev. Lett. **85**, 98 (2000).
10. S. M. Zakharov, G. V. Ivanenkov, A. A. Kolomenskiĭ, *et al.*, Pis'ma Zh. Tekh. Fiz. **9**, 1192 (1983) [Sov. Tech. Phys. Lett. **9**, 512 (1983)].
11. E. Grabovsky, K. Mitrofanov, G. Oleinik, *et al.*, in *Proceedings of the European Conference on Advanced Diagnostics for Magnetic and Inertial Fusion, Varenna, 2001*, Ed. by P. E. Stott *et al*. (Kluwer, New York, 2001), p. 419.
12. V. V. Alexandrov, M. V. Fedulov, I. N. Frolov, *et al.*, in *Proceedings of the 5th International Conference on Dense Z-Pinches, Albuquerque, 2002*, p. 91.
13. G. S. Volkov, E. V. Grabovskiĭ, I. Yu. Porofeev, *et al.*, Preprint No. 0104A (Troitsk Institute for Innovation and Fusion Research, Troitsk, 2003).
14. V. V. Gavrilov, Doctoral Dissertation (Troitsk, 1999).
15. Z. A. Al'bikov, V. P. Belik, S. V. Bobashev, *et al.*, *Plasma Diagnostics*, Ed. by M. I. Pergament (Énergoatomizdat, Moscow, 1989).
16. A. Alexandrov, A. Branitskii, E. V. Grabovskii, *et al.*, in *Inertial Fusion Sciences and Applications 99*, Ed. by C. Labaune, W. J. Hogan, and K. A. Tanaka (Elsevier, St. Louis, 1999), p. 591.
17. T. A. Shelkovenko, S. A. Pikuz, D. B. Sinars, *et al.*, IEEE Trans. Plasma Sci. **30**, 567 (2002).
18. A. V. Branitskii, E. V. Grabovskii, M. V. Frolov, *et al.*, in *Proceedings of the 12th International Conference on High-Power Particle Beams, Haifa, 1998*, p. 599.
19. V. V. Aleksandrov, A. V. Branitskiĭ, G. S. Volkov, *et al.*, Fiz. Plazmy **27**, 99 (2001) [Plasma Phys. Rep. **27**, 89 (2001)].
20. V. V. Aleksandrov, E. V. Grabovskiĭ, G. G. Zukakishvili, *et al.*, Zh. Éksp. Teor. Fiz. **124**, 829 (2003) [JETP **97**, 745 (2003)].
21. E. V. Grabovskiĭ, G. G. Zukakishvili, S. L. Nedoseev, *et al.*, Fiz. Plazmy **30**, 33 (2004) [Plasma Phys. Rep. **30**, 30 (2004)].
22. V. V. Aleksandrov, G. S. Volkov, E. V. Grabovskiĭ, *et al.*, Fiz. Plazmy **30** (3) (2004) (in press).

Translated by N.N. Ustinovskiĭ